

The Manufacturing Engineering Society International Conference, MESIC 2013

## Experimental Study on the Evaluation of Necking and Fracture Strains in Sheet Metal Forming Processes

G. Centeno<sup>a,\*</sup>, A. J. Martínez-Donaire, C. Vallellano, L. H. Martínez-Palmeth,  
D. Morales, C. Suntaxi, F. J. García-Lomas

<sup>a</sup> *Department of Mechanical and Materials Engineering. University of Sevilla. Camino de los Descubrimientos s/n, 41092 Sevilla, Spain.*

---

### Abstract

In this paper the formability of AA2024-T3 metal sheets is experimentally analyzed. For this purpose, a series of Stretch-Bending and Incremental Sheet Forming (ISF) tests are carried out. The former tests allow determine the formability limits through the evaluation of necking and fracture using the optical deformation measurement system ARAMIS<sup>®</sup> and measuring the thickness strains along the fracture line. The latter are performed with the aim of confirming the validity of these limits. In this case, the spifability, formability in Single Point Incremental Forming (SPIF), was studied in the light of circle grid analysis by means of the 3D deformation digital measurement system ARGUS<sup>®</sup>. Different punch diameters are used in both processes. The results exhibit the importance of the accuracy in the setting of the formability limits as well as the variability that these limits present depending on the forming process or some variables such as the tool radius.

© 2013 The Authors. Published by Elsevier Ltd. Open access under [CC BY-NC-ND license](https://creativecommons.org/licenses/by-nc-nd/4.0/).

Selection and peer-review under responsibility of Universidad de Zaragoza, Dpto Ing Diseño y Fabricacion

*Keywords:* Formability limits; Stretch-Bending; Incremental Sheet Forming (ISF); Single Point Incremental Forming (SPIF).

---

---

\* Corresponding author. Tel.: +34-9-54 48 -5965; fax: +34- 9-5446- 0475.

*E-mail address:* [gaceba@us.es](mailto:gaceba@us.es)

## 1. Introduction

The AA2024-T3 is a thermally treated Aluminium Alloy widely used in the manufacture of aircraft structures, especially wing and fuselage skins under tension. So, in order to avoid production problems and to optimize the forming processes it is essential to establish accurate formability limits. In this sense, the Forming Limit Diagram (FLD) is the most useful tool for evaluating the workability of sheet metals. They show, in the principal strain space, the combinations of strains at the onset of local necking, FLD at necking or FLC (forming limit curve), and at the beginning of ductile fracture, FLD at fracture or FFL (forming fracture line).

High ductility materials usually start the failure process with the onset of strain localization along a narrow stripe, leading to the formation of a neck (necking). The material deforms continuously within this neck, following approximately a near plane strain state, until the ductile fracture takes place. On the contrary, for low ductility materials the fracture may occur in absence of the necking process, being the formability of the sheet controlled by ductile fracture mechanisms. The Fig. 1 depicts the formability limits, by means of the FLD at necking and fracture, for high-ductility and for low-ductility materials, which is in fact expected in the case of the AA2024-T3 1.2 mm thickness metal sheets, considering previous experimental results such as Vallellano et al. (2008) and Centeno et al (2012a).

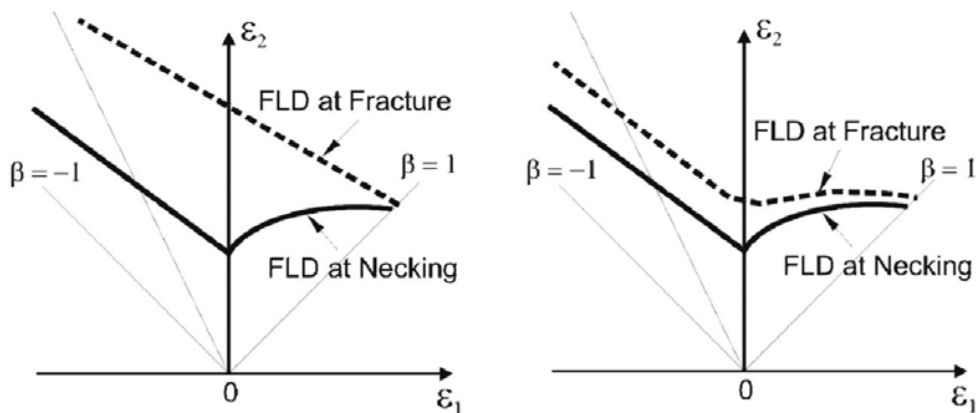


Fig. 1. FLD at necking and at fracture for high-ductility (left) low-ductility (right) materials.

The occurrence of fracture in absence of necking is more likely to occur in stretching operations, especially within near equi-biaxial conditions, where the sheet undergoes a biaxial strain state (see Fig. 1), and in incremental forming operations under certain forming conditions characterised by small punch diameters and step downs. Such facts add an extra complexity to the analysis of failure.

In addition, recent studies show that the local evolution of the stress/strain gradient through the sheet thickness is essential to explain the bending effect in formability, focusing mainly on the strains of both the inner and the outer surfaces at the process zone of the metal sheet. In fact, depending on the severity of the strain gradient, two types of failures can be expected: (1) a Necking-Controlled Failure, which takes place when the entire sheet thickness becomes plastically unstable; and (2) a Fracture-Controlled Failure, which arises when the outer surface of the sheet fracture. In this way, in ISF processes failure changes from type (1) to (2) as the radius of the forming tool decreases. In fact, some recent studies allow conclude that the failure mode above described clearly depends on the parameter  $t_0/R$ , ratio of the initial sheet thickness  $t_0$  to the radius of the forming tool  $R$ , as pointed out for instance by Stoughton and Yoon (2011), and Vallellano et al. (2010) in stretch-bending, and by Silva et al. (2011) in the case of SPIF. In this sense, the authors also suggested in Centeno et al. (2012b) the importance of quantifying the enhancement of formability in ISF due to the bending effect by means of this  $t_0/R$  ratio.

In this paper the feasibility of fracture limits for AA2024-T3 metal sheets is discussed. For this purpose, a series of stretch-bending and Single Point Incremental Forming (SPIF) tests are carried out. The stretching and stretch-bending tests permitted to determine the conventional formability limits through the evaluation of necking and fracture. The SPIF tests were performed with the aim of confirming the verisimilitude of these limits. The results exhibit the importance of the accuracy in the setting of the formability limits as well as the variability that these limits present depending on the forming process or some variables such as the tool radius.

## 2. Experimentation

In order to obtain and discuss the formability limits of the AA2024-T3 sheets, a series of stretch-bending and single point incremental forming tests have been carried out. The methodology followed to obtain the formability limits for each case is exposed in this section.

### 2.1. Stretching and stretch-bending tests

A series of Nakazima tests (hemispherical punch of  $\text{Ø}100$  mm) have been carried out using three different specimen geometries with the aim of obtaining the conventional forming limits, represented by the FLC and the FFL as discussed above. The Nakazima tests were performed in a universal sheet metal testing machine Erichsen 142-20 (see Fig. 2), being the testing conditions taken according to the ISO standard 12004-2 (2008). The punch velocity was set to 1 mm/s and the lubricant at the interface punch-sheet was Vaseline + PTFE + Vaseline.

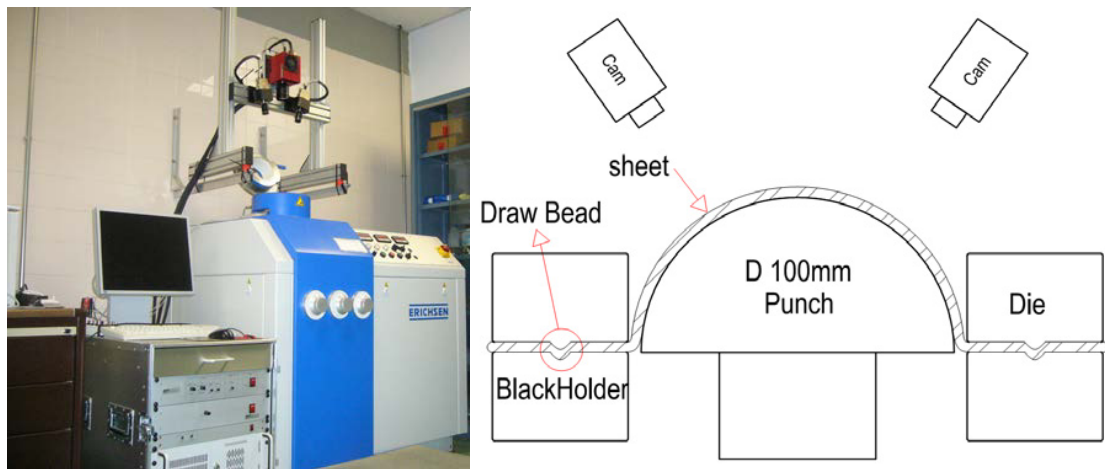


Fig. 2. Universal sheet metal testing machine (left) and a scheme of the experimental setup (right).

The optical deformation measurement system ARAMIS<sup>®</sup>, based on digital image correlation technique, was utilized to evaluate along the tests the strain distributions at the outer surface of the sheets by following the methodology explained in Martínez-Donaire et al. (2008). For the whole Nakazima testing plan, the material presented a fracture-controlled failure, i.e. all the metal sheets failed directly by fracture in absence of a distinctive necking. Considering this behavior, two failure curves were set: (1) the Engineering Fracture Line (EFL) and (2) the Fracture Forming Line (FFL).

The EFL was obtained by measuring the characteristic major and minor strains around the failure zone at the last image recorded by ARAMIS<sup>®</sup> just before the crack appearance (see Fig. 3). In the present case, the EFL would almost coincide with the FLC at necking calculated by using the ISO standard 12004-2 (2008) for this material.

This can be explained by the small calculating window around the fracture line corresponding to the behavior of this material (for more details see Martínez-Donaire et al., 2010).

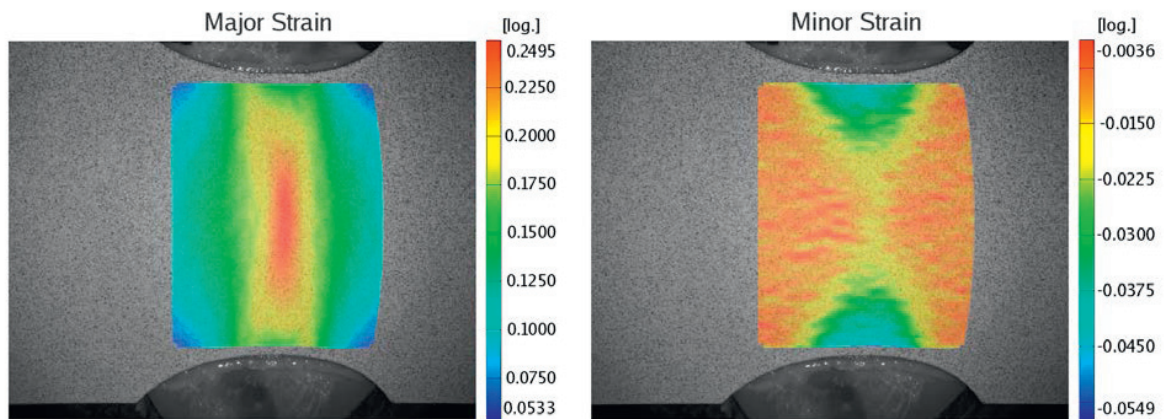


Fig. 3. Contour of major (left) and minor strains (right) at last image before the crack appearance in a Nakazima test near plane strain conditions.

On the other hand, the Fracture Forming Line (FFL), which for this low-ductility material does not appear as a straight line, was evaluated by following the principles explained in Silva et al. (2011). The procedure for constructing the FFL starts by measuring the thickness at fracture at several places along the crack in order to obtain the average thickness strain, as shown in Fig. 4 (left). Average thickness strain was evaluated at both sides of the crack for every tested metal sheet. In addition, some tested sheets were cut and the thickness was measured from a profile view, as shown in Fig. 4 (right), in order to validate the previous thickness measurements along the crack.

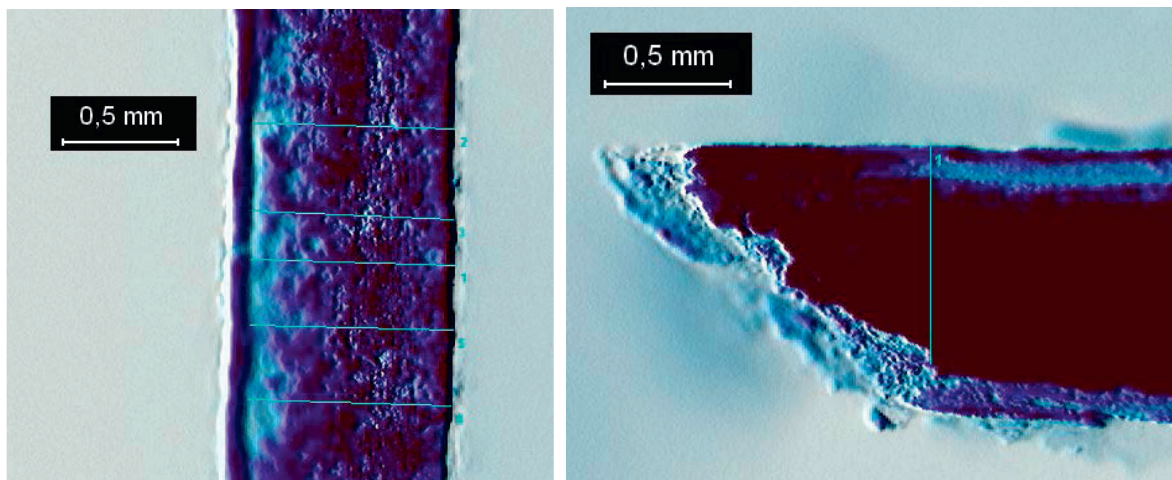


Fig. 4. Average thickness measurement along the crack (left) and validation from a profile view (right).

The average minor strain was evaluated along the fracture line at the last image recorded by ARAMIS® just before the crack appearance. Finally, major strain was calculated by volume constancy:

$$\bar{\varepsilon}_{1,f} = -(\bar{\varepsilon}_{2,f} + \bar{\varepsilon}_{3,f}) \quad (1)$$

Finally, the application of the same methodology for evaluating fracture to previous stretch-bending tests (whose results can be found in Centeno et al., 2012b), carried out by using cylindrical punch diameters of  $\phi 20$ , 12 and 10 mm, allowed verifying the likely enhancement of formability due to the bending effect by means of  $t_0/R$  ratio. The specimen geometry for those tests was chosen in order to obtain a deformation state near plane strain, which also occurs in SPIF.

## 2.2. Single point incremental forming tests

A series of SPIF tests were carried out within the experimental plan exposed in Table 1. The setup described in Pérez-Santiago et al. (2011) was used to perform the tests following this testing methodology. The geometry was a conical frustum with circular generatrix, with the initial diameter of the truncated cone set to 70 mm, being the initial drawing angle  $20^\circ$  and the generatrix radius 40 mm. The step down was set to 0.2 mm per pass. Tool diameters of 10 and 20 mm were used. The rotation of the tool was free and the feed rate used for all tests was set to 3000 mm/min. Special lubricant Houghton TD-52 for metal forming applications was used in order to minimize friction effects. The final depth and final forming angle were recorded just in the instant in which the failure took place. Three replicates of each SPIF test were carried out in order to provide statistical meaning to the results. As can be observed in Table 1, almost the same final depths, and consequently final forming angles, were repetitive achieved for each case.

Table 1. Series of SPIF tests carried out

Tool diameter $\phi_T$ (mm)	Final depth $Z_f$ (mm)	Final forming angle $\alpha_f$ (mm)
20	13.4 / 13.4 / 13.4	52.79 / 52.79 / 52.79
10	14.4 / 13.8 / 13.8	54.57 / 53.51 / 53.51

The strain state was measured in the light of circle grid analysis, within a similar methodology to that latterly performed in Centeno et al (2012c), by using the 3D deformation digital measurement system ARGUS®. With this aim, a point pattern had to be created on every undeformed sheet blank by an electrolytic etching process. The Fig. 5 (left) depicts the point pattern after deforming a metal sheet by SPIF until failure with a hemispherical forming tool of 10 mm diameter. This analysis provides the contour of principal strains at the outer surface of the final part, as shown in Fig. 5 (right). As said before, this was performed using the commercial software ARGUS®. As can be seen, the area of maximum logarithmic major strain is obviously located at the vicinity of the crack (notice that orientation of the final part coincides in Fig. 5 left and right).

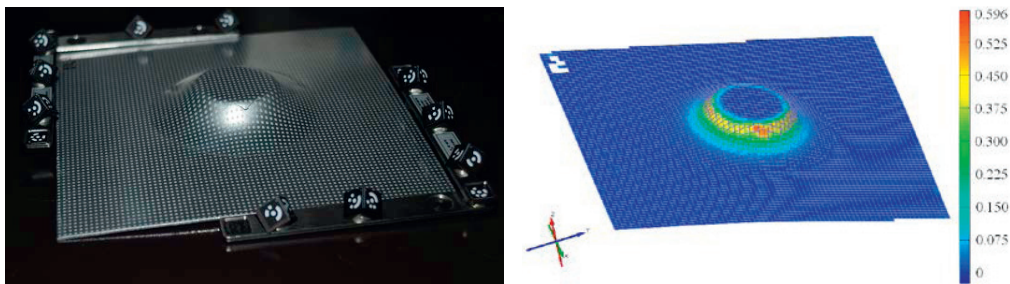


Fig. 5. Point pattern (left) and contour of major true strains (right) after SPIF test obtained by ARGUS®.



It must also be observed that the crack develops from a certain depth at the forming wall having an upward development to both sides, which was accurately captured by the measurement system. In fact, the measurement system was able to measure the deformation of the ellipses both above and below it, and therefore able to interpolate the strains throughout the crack, providing the continuous contour map as depicted in Fig. 5 (right). As has been commonly observed, as for example in Silva et al. (2011) and Centeno et al. (2012c), metal sheets formed by incremental forming present a trend of principal strains within the forming limit diagram (FLD) that grows in the first quadrant towards failure close to plane strain condition. In fact, the Fig. 6 depicts the principal strains at the FLD of the previous final part formed by SPIF corresponding to the colored contour of major strain represented in Fig. 5 (right).

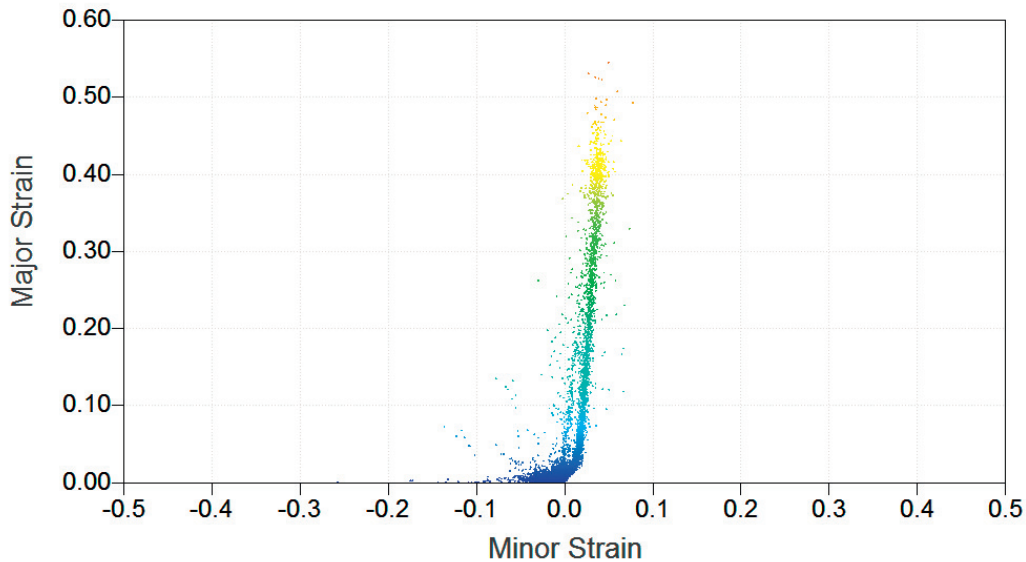


Fig. 6. Principal strains at the FLD of the final part formed by SPIF.

At this point it must be said that the points corresponding to the maximum level of major strains, those in red at Fig. 6, are processed by ARGUS<sup>®</sup> as mentioned above by means of an interpolation throughout the crack. In this sense, these points might represent the level of principal strains at fracture with certain feasibility. Nevertheless, the validity of these fracture strains must be verified with microscopic measurements. In fact, both the formability and the fracture strains were verified using microscopic thickness measurements by applying the same methodology that was previously used with the stretch-bending tests. Actually, sheet thickness at fracture was measured at several places around the final part formed in SPIF. As can be seen in Fig. 7 (left), the average thickness strain was evaluated at both sides just where the crack occurs, and therefore the average major strain at fracture was calculated. This evaluation was also carried out at the opposite wall with respect to that where the crack appears, as can be seen in Fig. 7 (right), in order to validate the higher levels of achievable principal strains, corresponding to the points colored in yellow and orange in Fig. 6.

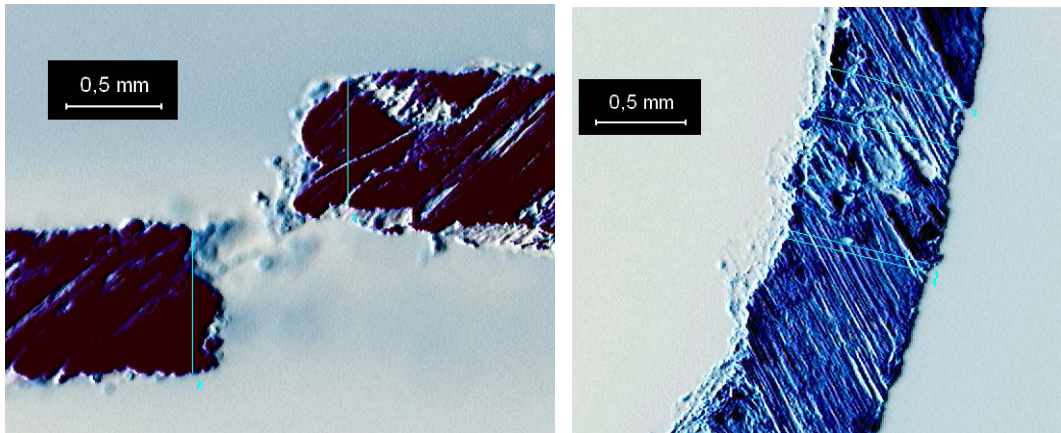


Fig. 7. Thickness measurement in SPIF at the crack location (left) and opposite of it (right).

### 3. Results and discussion

Based on the results of the series of Nakazima tests corresponding to the three different specimen geometries utilized (i.e. uniaxial, plane strain and biaxial strain), and using the fracture strains calculated respectively by ARAMIS<sup>®</sup> and from thickness measurements at the microscope, the conventional forming limits EFL and FFL are constructed. Finally, the Fig. 8 depicts the EFL and the FFL in a range of minor strains from -0.15 to 0.05 approximately. As can be seen, the EFL presents a straight evolution while the FFL seems to present the V-shape evolution expected for this kind of low-ductility materials, as was mentioned above.

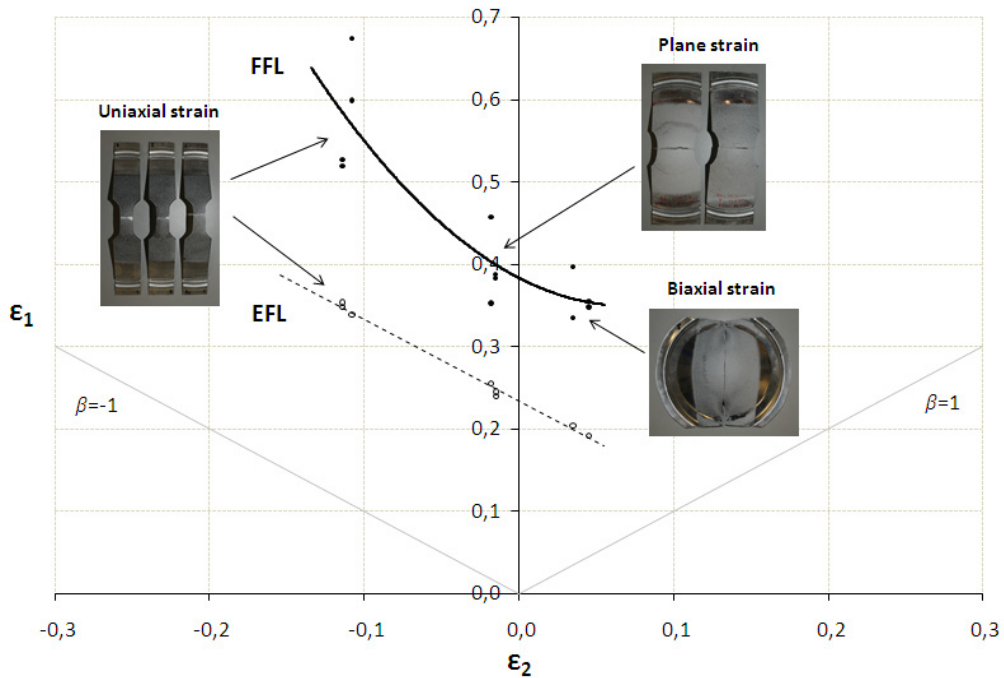


Fig. 8. Conventional formability limits EFL and FFL.

On the contrary, the level of major strains at fracture within the FFL at the first quadrant and close to plane strain condition differs to those formability levels shown in Fig. 6 for the case of SPIF. In any case, the validity of this fracture curve must be checked against other forming processes, such as the case of SPIF or stretch-bending by using small cylindrical punches. Actually, fracture strains, evaluated by measuring thickness at the microscope, for the highest formability corresponding to both series of SPIF and stretch-bending tests respectively (which in both cases coincides with the smallest forming tool considered, i.e. a forming tool of 10 mm diameter) are represented in Fig. 9. First of all, for the case of SPIF, the fracture strains calculated by applying this methodology are consistent with those registered by ARGUS<sup>®</sup> for the same case. Moreover, it can be easily noticed that this fracture strains are well above the FFL. It is well known that in the case of ductile materials, failure strains are above the FLC, being failure controlled by fracture with absence of necking, as discussed for instance in Silva et al. (2011) and Centeno et al. (2012c). In those cases, and depending on certain process parameters, the metal sheet deformed by SPIF could increase formability until the FFL. But the phenomenon captured for this low-ductility aluminum alloy consists on an upward displacement of the fracture limit of the metal sheet when it is deformed by SPIF.

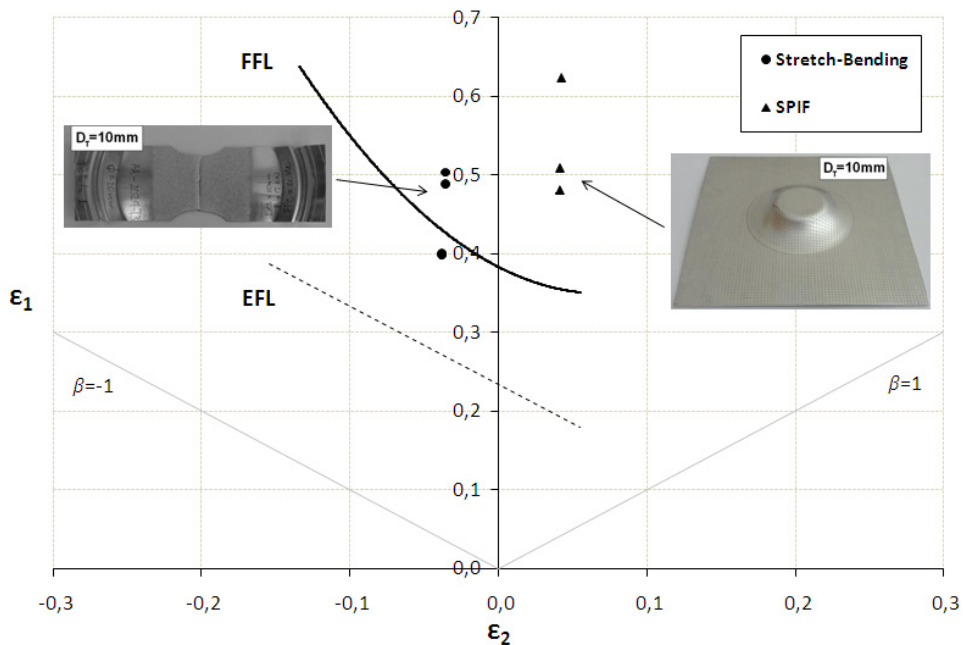


Fig. 9. Fracture strains in SPIF and Stretch-bending for a tool diameter of 10mm.

Two interesting results can be pointed out from Fig. 9. On the one hand, it can be seen that the fracture strains in the Stretch-bending tests with cylindrical punch of 10 mm diameter are quite similar to that obtained with Nakazima tests (FFL), and only in some cases placed slightly above this fracture limit. This denotes a relatively insensitivity of fracture strains with the bending effect for this material, in which failure is mainly controlled by the maximum shear stresses, as discussed in Vallellano et al. (2008). On the other hand, it has been found that fracture strains in SPIF are clearly above both the FFL and as well above the fracture strains in Stretch-bending. This seems to indicate that the enhancement on formability obtained with SPIF might not be only explained via the effect of bending induced by the tool radius. Other parameters such as shear stresses, the contact stresses, the cyclic straining and the hydrostatic stresses Emmens and den Boogaard (2009) may be affecting the overall spifability of the AA2024-T3. The analysis of these parameters individually would require a detailed experimental and numerical study to characterize the effect of each one of these variables independently.



#### 4. Conclusions

This paper analysed experimentally the formability of AA2024-T3 metal sheets under different forming processes: stretching, Stretch-bending and single point incremental forming. The conventional formability limits were correctly set from a series of normalized Nakazima tests by using different specimen geometries. The feasibility of these conventional forming limits, and especially the fracture forming curve, was put to the test by evaluating the failure strains of stretch-bending and SPIF experiments carried out using tool of relative small diameters.

The results seem to show that the bending effect, controlled by the  $t_0/R$  ratio, might not be enough to explain the enhanced formability registered in SPIF. In this sense, other parameters should be pointed out to have an influence in the phenomenon captured in relation with the spifability of this low-ductility aluminium alloy. In any case, the authors would propose a more insistent experimental plan in order to further analyze this phenomenon, their causes and to fully confirm its experimental occurrence.

#### Acknowledgements

The authors would like to thank the Spanish Government for its financial support through the Project No. DPI 2009-13335. The authors would also like to thank to GREP at the University of Girona, especially to I. Bagudanch and M.L. Garcia-Romeu, for borrowing their facilities to carry out the SPIF tests.

#### References

- Centeno, G., Vallellano, C., Vázquez, J., Morales, D., Martínez-Donaire, A.J., García-Lomas, F.J., 2012. Numerical analysis of the deformation mechanisms in incremental forming of AA2024-T3 sheets. AIP Conference Proceedings 1431, pp. 740-747.
- Centeno, G., Doblas, F.J., Martínez-Palmeth, L.H., Martínez-Donaire, A.J., Vallellano, C., 2012. FEA of the Bending Effect in the Formability of Metal Sheets via Incremental Forming. Steel Research International, Special Edition: 14th Metal Forming International Conference 2012, pp. 447-450.
- Centeno, G., Silva, M.B., Cristino, V.A.M., Vallellano, C., Martins, P.A.F., 2012. Hole-flanging by incremental sheet forming. International Journal of Machine Tools and Manufacture 59, pp. 46-54.
- Emmens, W.C., van den Boogaard, A.H., 2009. An overview of stabilizing deformation mechanisms in incremental sheet forming. Journal of Material Processing Technology 209, pp. 3688-3695.
- ISO 12004-2:2008, Metallic Materials-Sheet and Strip-Determination of Forming Limit Curves in Laboratory.
- Martínez-Donaire, A.J., Vallellano, C., Morales, D., García-Lomas, F.J., 2010. Experimental Detection of Necking in Stretch-Bending Conditions: a Critical Review and New Methodology. Steel Research International 81, pp. 781-784.
- Pérez-Santiago, R., Bagudanch, I., García-Romeu, M.L., 2011. Force Modeling in Single Point Incremental Forming of Variable Wall Angle Components. Key Engineering Materials 473, pp. 833-840.
- Silva, M.B., Nielsen, P.S., Bay, N., Martins, P.A.F., 2011. Failure mechanisms in single point incremental forming of metals. International Journal of Advanced Manufacturing Technology 56, pp. 893-903.
- Stoughton, T.B., Yoon, J.W., 2011. A new approach for failure criterion for sheet metals. International Journal of Plasticity 27, pp. 440-459.
- Vallellano, C., Morales, D., García-Lomas, F.J., 2008. A study to predict failure in biaxially stretched sheets of Aluminum alloy 2024-T3. Materials and Manufacturing Processes 23, pp. 303-310.
- Vallellano, C., Morales, D., Martínez-Donaire, A.J., García-Lomas, F.J., 2010. On the Use of Concave-Side Rule and Critical-Distance Methods to Predict the Influence of Bending on Sheet-Metal Formability. International Journal of Material Forming 3 S1, pp. 1167-1170.